3 Relaxation

The relaxation is one of the main properties characterising a paramagnetic spin system. In case of endohedral fullerenes, the coupling of the encapsulated spins with the surrounding is mediated by the fullerene molecule. Especially for $N@C_{60/70}$ and $P@C_{60}$, this coupling is very weak because of the lack of direct molecular bonds. Thus, long relaxation times can be expected.

After an excitation of the spin system two processes are involved in the relaxation of the magnetisation towards thermal equilibrium. The first describes the change of the entire magnetisation of the spin system through spin-phonon coupling and is therefore called spin-lattice relaxation. The time constant of this process is usually referred to as T_1. The second process only affects the phase coherence of the spins, e.g. as spin diffusion, and contains information about the coupling between spins. Usually this spin-spin relaxation time T_2 is much smaller than T_1, especially in solids at low temperatures when the lattice vibrations are frozen out. Only in rare cases in solution T_2 can equal T_1.

3.1   Experimental details

All samples discussed in this chapter are powder samples. The $P@C_{60}$ sample used for the temperature dependent measurements has been prepared from "as-produced" material dissolved in toluene, filtered once, and then dried in a rotational evaporator. The ratio of filled to empty cages is $2.4 \cdot 10^{-5}$ and corresponds to $2.0 \cdot 10^{13}$ spins/mg[6]. This sample will be referred to as "Phoenix".

The T_1 and T_2 relaxation times were measured in ESR pulse experiments. Both techniques are based on the Hahn-Echo sequence [1], a $\pi/2$–pulse followed by a π–pulse applied along the same axis (Fig. 3.1).
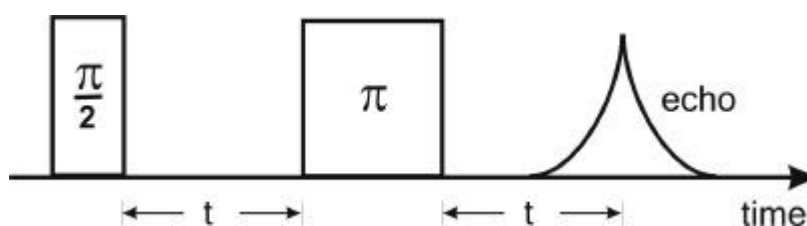

*Fig. 3.1: pulse scheme of a Hahn - Echo sequence. A typical value for a **p** -pulse is 32 ns, and ~1 µs for the time t between the pulses.*

The effect of this pulse sequence on the spins is illustrated in Fig. 3.2. The magnetisation along the z–axis is tipped through 90° by application of B_l along the y–

---

[6] The error of absolute spin numbers is always quite high (at least a factor 2) because no spin standard is similar enough to the material investigated concerning g-factor, linewidth etc.

axis (a). The spins start to dephase coherently due to static inhomogeneities (b), e.g. due to inhomogeneities of B_0. After a time t they are refocused by a π–pulse (c-e) before dephasing again after a time $> 2t$ (f).

The spin–spin relaxation time is measured by changing the time t between the pulses while recording the echo–intensity. For the measurement of the spin–lattice relaxation, a π–pulse inverting the z–magnetisation is applied before the Hahn–Echo sequence. While varying the time between this inversion pulse and the following two pulses (t = const), again the echo intensity is observed thus measuring the relaxation of the magnetisation towards thermal equilibrium. This experiment is called inversion recovery.
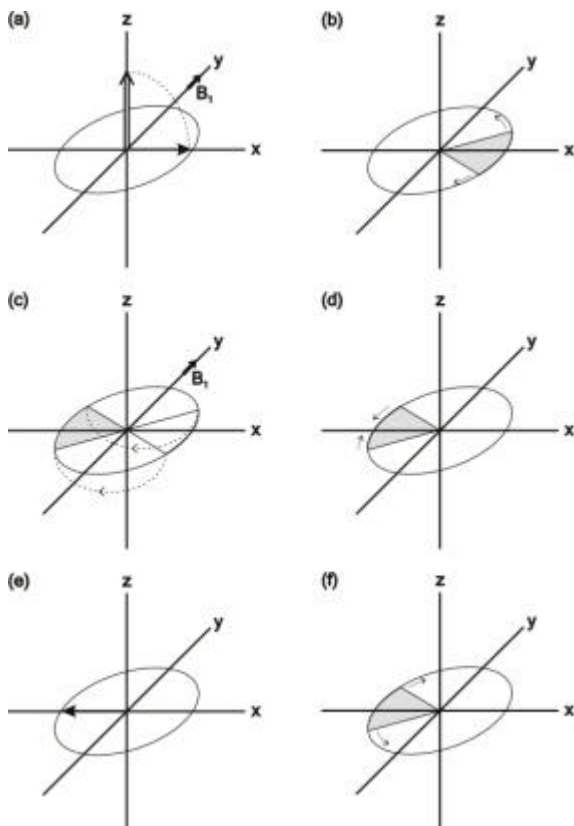

Fig. 3.2: *The Hahn spin–echo experiment as described in the text. The first pulse, e.g. applied along the y–axis as in (a), rotates the z-magnetisation to the x–axis. (b)Due to static inhomegeneities the spins start to dephase coherently in the x,y-plane. (c) At a time t after the first pulse, the second pulse is applied and rotates the spins by 180°. (d,e) After the second waiting time t the spins are refocused at the (-x)–axis before dephasing again (f), thus forming an echo with the magnetisation measured along the x–axis.*

3.2   Spin – lattice relaxation

Both, the absorption (real part) and dispersion (imaginary part) of the magnetisation, can be measured with quadrature–detection. If the first shows the echo amplitude, the latter should be zero throughout the experiment corresponding to the signal noise. In

Fig. 3.3 the real part (a) and the imaginary part (b), blue line, of the echo amplitude of the inversion recovery experiment at $T = 100$ K are shown.

The real part of the data has been fitted with both a single and a double exponential function. The corresponding residua are shown in Fig. 3.3 (b) as black (single exponential) and red line (double exponential). The imaginary amplitude (blue line) of the echo is shifted for better illustration. It corresponds to the signal noise and is therefore an indicator for phase– and frequency shifts occurring during the measurement. The units are referred to as "counts". This is to point out that the fit residua have the same scaling as the data and should follow the signal noise if the fit were valid.

As can be seen, only the fit with $f(t) = a + b \cdot exp(-t \cdot R_1) + b \cdot exp(-t \cdot R_2)$ yields a residuum that varies by 0.35 counts just as the imaginary amplitude does. In contrast, the residuum of a single exponential fit (black) shows a clear structure with a large variation from the signal noise especially for short times (2.25 counts).
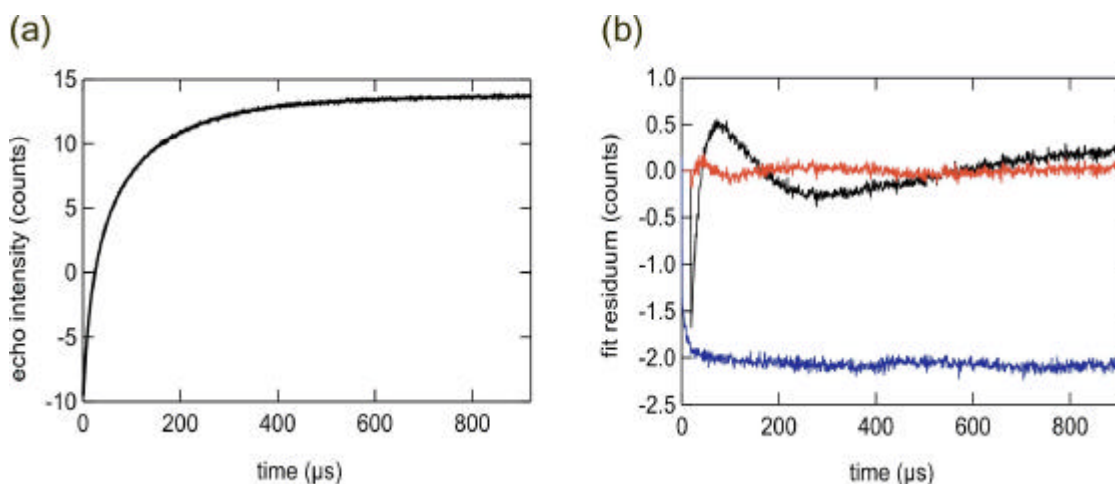

Fig. 3.3:(a) Echo amplitude measured in an inversion recovery experiment at T = 100 K.

(b)The residua of the spin-lattice relaxation at T = 100 K fitted with a single exponential (black) and a double exponential function (red) show that relaxation of the inverted magnetisation towards equilibrium cannot be described by a single exponential decay. The imaginary amplitude of the echo is shifted by –2.0 counts for better illustration (blue) and should be constant throughout the experiment. It corresponds to the signal noise and is therefore an indicator for phase- and baseline shifts occurring during the measurement.

A deviation from the single exponential relaxation of the magnetisation is reported also for ^{14}N@C$_{60}$ (T < 100 K) [2] and ^{15}N@C$_{60}$ [3]. This phenomenon can originate from different relaxation rates for the ($\pm 3/2$, $\pm 1/2$) and (1/2, – 1/2) transitions, respectively. This idea is further examined in chapter 4.4 using the method of transient nutation.

If the relaxation experiments are evaluated with a double exponential function as described before, two relaxation rates are obtained. The temperature dependence of the two spin–lattice relaxation rates is shown in Fig. 3.4 (a). At temperatures T = 250 K, the relaxation of the magnetisation shows only single exponential characteristics indicating

that the phase transition of C_{60} has an influence on the relaxation properties of the endohedral spin. Apart from some variation R_1 and R_2 seem to have a fixed ratio, and the temperature dependence of the two components is the same. This implies that there are two relaxation processes which arise from the same origin.
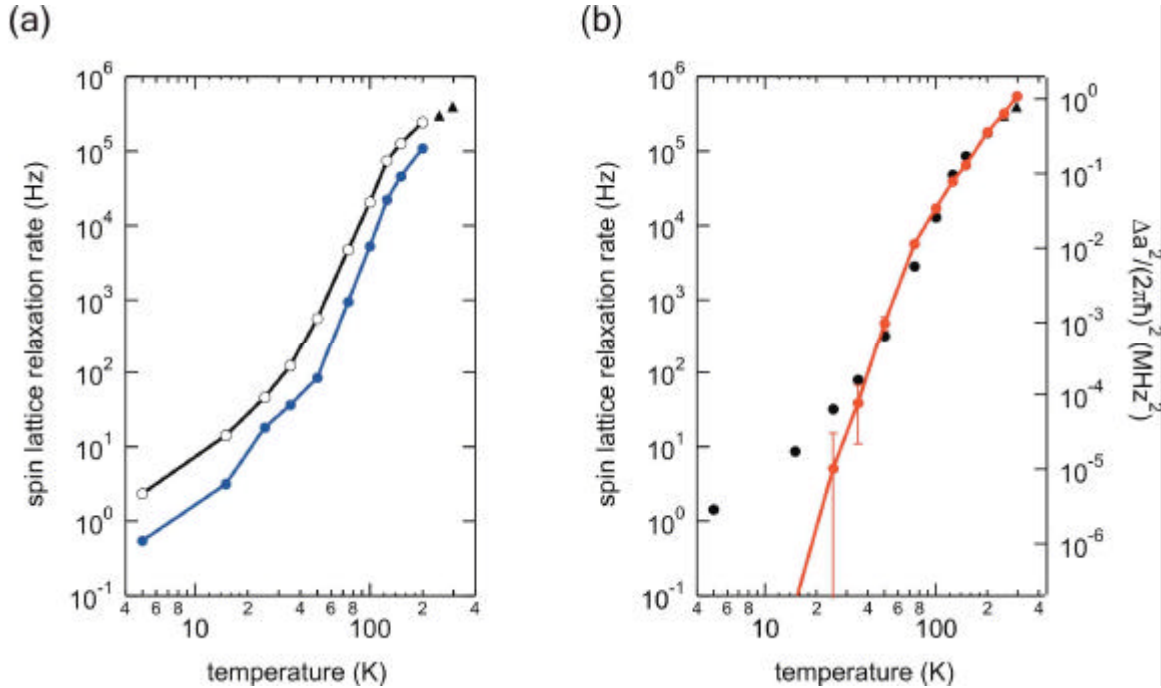

Fig. 3.4(a) *Temperature dependence of the two spin-lattice relaxation rates R_1 (black open markers) and R_2 (blue solid markers) evaluated as described in the text. For $T \geq 250$ K only one relaxation rate is observed (black triangles).*

(b)Temperature dependence of the mean relaxation rate R_{mean} (black markers) compared to the fluctuations of the hyperfine coupling yielded from the temperature dependence of the hyperfine coupling (explanation see text).

In Fig. 3.4 (b) the mean relaxation rate $R_{mean} = (R_1 + R_2)/2$ is compared to the mean square amplitude of the hyperfine fluctuation $\Delta a^2(T) = (a(T)/2\pi h - a_0/2\pi h)^2$ with data $a(T)/2\pi h$ taken from the measurement presented in chapter 2, which yielded a ground state hyperfine coupling constant $a_0/2\pi h = 137.32$ MHz. The comparison with R_{mean} is justified because the temperature dependence of the two relaxation rates is the same. It can be clearly seen that the temperature dependence is the same for R_{mean} and Δa^2 within the error bars for $T > 35$ K indicating that the vibration of the endohedral atom is the main source of relaxation.

We will now have a closer look at the Hamiltonian of the system because the relaxation is due to its fluctuating fields. The Zeemann term does not contribute because changes of B_0 are homogeneous over the entire sample and therefore coherent. However, coherent fluctuations do not cause relaxation [4].

Interactions that can cause relaxation are the hyperfine coupling H_{hf}, the fine structure coupling H_{fs}, and dipolar couplings H_{dip} to other nuclear or electron spins. Exchange

coupling will not be considered here, as the spin density on the fullerene cage is small. With these assumptions the spin Hamiltonian relevant for relaxation reads as

$$H_{rel} = H_{hf} + H_{fs} + H_{dip}$$
$$= \mathbf{IAS} + \mathbf{SDS} + \mathbf{STR} \tag{3.10}$$

where R is a ^{13}C nuclear spin, or (depending on the concentration) the next endohedral electron spin.

All these couplings depend on relative lattice co-ordinates. Therefore they can be modulated by phonons and give rise to spin–lattice relaxation. In Fig. 3.5 the relevant phonon modes for group V endohedral fullerenes in a C_{60} matrix are visualised.
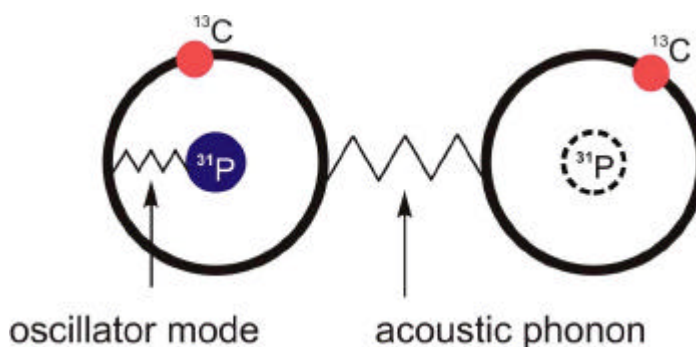

Fig. 3.5:   *Scheme of the phonon modes that are relevant for relaxation. The oscillator or "inner" mode modulates the dipolar coupling to a ^{13}C nuclear spin on the endohedral fullerene. Since the wavefunction of the endohedral atom is squeezed, this vibration also modulates the hyperfine and fine structure coupling. The acoustic or "outer" mode modulates the dipolar coupling between an endohedral electron spin and neighbouring ^{13}C nuclear spins or another endohedral spin.*

The "inner" mode, where the endohedral atom vibrates inside the fullerene molecule, is described by a harmonic oscillator. This is evidenced by the temperature dependence of the hyperfine coupling. As shown in chapter 2, the ground state energy of this oscillator is $E_0 \sim 15$ meV. The internal oscillation can also modulate the dipolar coupling to a ^{13}C nuclear spin on the endohedral fullerene[7], and since the wavefunction of the endohedral atom is squeezed, this vibration modulates the hyperfine and fine structure coupling as well.

On the other hand, acoustic phonons can modulate the dipolar coupling to ^{13}C nuclear spins on neighbouring fullerene molecules, and they change the dipolar coupling between two endohedral electron spins. The van der Waals forces between the fullerenes induce a non–spherical charge distribution on the molecules that causes a fine structure splitting of the endohedral spin (see chapter 5). Lattice vibrations can modulate the van der Waals forces and therefore the charge density on the endohedral

---

[7] With the natural abundance of 1.11% for the ^{13}C isotope, every second fullerene molecule contains at least one ^{13}C atom.

fullerene. With this, in addition to the dipolar coupling, the fine structure coupling might be modulated as well.

As shown in Tab. 3.1, the hyperfine and finestructure couplings are stronger by more than one order of magnitude compared to the dipolar coupling to a ^{13}C nuclear spin R on the same fullerene molecule. Furthermore, this dipolar coupling is averaged out for temperatures T > 80 K due to rotations of the C_{60}. Thus, A and D will dominate the relaxation process in the case of the internal oscillator.

The strength of the interactions modulated by acoustic phonons is strongly angle dependent as all interactions are dipolar couplings with $T(\vartheta) = T_0 \cdot 1/2 \cdot (3\cos^2\vartheta - 1)$. For comparison the couplings have been calculated for $\vartheta = 0°$. The dipolar coupling is proportional to r^3, where r the distance between the spins. The shortest distance possible between an endohedral spin S and a ^{13}C spin R' on a neighbouring fullerene molecule is r = 7.5 Å. This value was used calculating the maximum strength of this specific coupling.

Tab. 3.1: Hamiltonian and coupling strength for different types of spin interactions. S and I are the electron and nuclear spin of the endohedral atom. R and R' are the nuclear spins of a ^{13}C on the same and neighbouring fullerene molecule. S' is the next endohedral electron spin. The dipolar interactions D and T depend on the angle ϑ of their main axis with respect to the magnetic field B_0.

oscillator mode	H_{int}	max. coupling strength ($\vartheta = 0°$)	phonon model
internal oscillator	**SAI**	$a/2\pi h \sim 140$ MHz	harmonic oscillator
	SDS	$D/2\pi h \sim 14$ MHz	
	STR	$T/2\pi h \sim 440$ kHz	
acoustic phonon	**STS'** [a]	$T/2\pi h \sim 50$ MHz	Debye
	STS' [b]	$T/2\pi h \sim 1$ kHz	
	STR'	$T/2\pi h \sim 70$ kHz	

[a] spin concentration 100 %

[b] spin concentration of "Phoenix"

For the sample "Phoenix" examined in this chapter, the dipolar coupling between S and R' is 70 times stronger than the coupling to the next endohedral spin. But with increasing spin concentration, dipolar couplings between endohedral electron spins S and S' will grow stronger and dominate the relaxation process. In samples with a spin concentration of about 0.2% the coupling of the endohedral spin to S' and R' will be of same strength.

For all samples investigated in this work, fluctuations of the hyperfine and finestructure coupling are the main relaxation mechanisms. We will now examine, how these mechanisms are described in terms of relaxation rates.

The relaxation rate is proportional to the transition probability W_{kl} between two energy levels k and l that can be calculated using Fermi's golden rule. It is

$$W_{kl} = \frac{2p}{\hbar} \left| \langle l | H_{\mathrm{int}} | k \rangle \right|^2 \cdot F(w) \qquad (3.11)$$

with the density of final states $F(w)$, that in our case corresponds to the phonon density of states. $F(w)$ is a delta function in the case of a harmonic oscillator and given by the Debye model in case of the acoustic phonons.

The hyperfine coupling gives rise to relaxation only between the two hyperfine states $M_I = +1/2$ and $M_I = -1/2$ due to its isotropic character as can be seen from the expansion

$$H_{hf} = a \left\{ I_z S_z + \frac{1}{2} [I_+ S_- + I_- S_+] \right\}. \qquad (3.12)$$

Relaxation between energy levels within one hyperfine state is caused by the fine structure Hamiltonian

$$\begin{aligned} H_{fs} = D_z \Bigg\{ &\frac{1}{2} \left(\cos^2 J - 1 \right) \cdot \frac{1}{2} \left[3S_z^2 - \mathbf{S} \cdot \mathbf{S} \right] \\ &+ \frac{3}{2} \sin J \cos J \cdot \frac{1}{2} \left[S_z S_+ + S_+ S_z + S_z S_- + S_- S_z \right] \\ &+ \frac{3}{4} \sin^2 J \cdot \frac{1}{2} \left[S_+^2 + S_-^2 \right] \Bigg\}. \end{aligned} \qquad (3.13)$$

As described in general by Mehring in [5] and pictured in Fig. 3.6, these relaxation paths of an eight level system give rise to two different relaxation rates R_{hf} and R_{fs}.
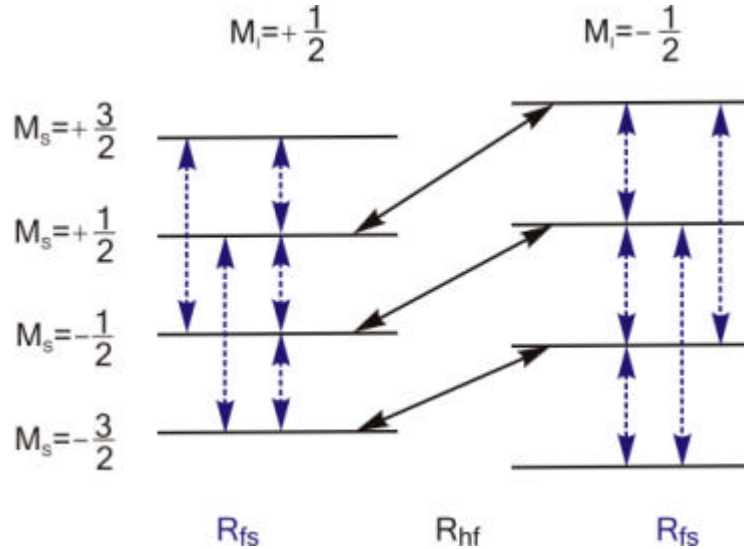

Fig. 3.6: Relaxation paths corresponding to the relaxation rates R_{hf} (solid arrows) and R_{fs} (dashed arrows). They have their origin in fluctuations of the hyperfine and fine structure Hamiltonian as described in the text.

As can be seen when these equations are inserted into equation (3.11), the relaxation rates obtained from the transition probabilities are

$$R_{hf} \propto \Delta a^2 \text{ and } R_{fs} \propto \left\langle D_z^2 \right\rangle. \tag{3.14}$$

Thus, not only the hyperfine fluctuation Δa causes spin lattice relaxation, as reported for $N@C_{60}$ in [6], but also the fluctuation of the finestructure coupling D_z. The origin of the fluctuations of the hyperfine coupling are vibrations of the endohedral nitrogen atom in the fullerene shell as discussed in chapter 2.

These relaxation rates can be determined by measuring the relaxation of the magnetisation

$$m_z(t) = 1 - c \cdot f(t) = 1 - c \cdot f_{hf}(t) \cdot f_{fs}(t) \tag{3.15}$$

with c = 2 for an inversion recovery experiment. The relaxation function $f(t)$ consists of a hyperfine part

$$f_{hf}(t) = \frac{1}{40}\left\{29 + 10 \cdot \exp\left(-\frac{3}{2}R_{hf} \cdot t\right) + \exp\left(-2R_{hf} \cdot t\right)\right\} \tag{3.16}$$

and a fine structure part

$$f_{fs}(t) = \exp\left(-\frac{9}{5}R_{fs} \cdot t\right) \tag{3.17}$$

Thus, the double exponential decay of the signal is due only to fluctuations of the hyperfine interaction. But due to the constant contribution in equation (3.16), the hyperfine relaxation alone will never cause the system to reach thermal equilibrium. Thus, both relaxation mechanisms are needed to explain the experimental data.

The relaxation $m_z(t)$ as given in equation (3.15) has been evaluated at different temperatures yielding the two relaxation rates as shown in Fig. 3.7 (a). These rates are very similar to those in Fig. 3.4 (a), where the data have been fitted with a heuristic double exponential function. Though we cannot decide which function fits the data better (as it is always the problem with multi–exponential functions), it is clear that the relaxation rates have the same temperature dependence as the fluctuation of the hyperfine coupling constant Δa^2 (red line). Therefore we can say, that the "inner" mode which modulates the hyperfine and the finestructure coupling, dominates the relaxation process for 35 K < T < 300 K.

In Fig. 3.7 (b) the mean relaxation rate of $P@C_{60}$ is compared to the mean relaxation rate of $N@C_{60}$ calculated from the data in [2]. In the temperature regime where the model of the harmonic oscillator is valid, the relaxation rate is much larger for phosphorous as endohedral atom than for nitrogen. As the phosphorous atom is larger than the nitrogen, the fluctuation of the coupling is larger, due to the larger overlap of the atomic wavefunction with that of the fullerene molecule [7]. Therefore, it can be

said that the vibration of the endohedral atom is the dominating spin–lattice relaxation mechanism.

However, if it were the only relaxation mechanism, the spin–lattice relaxation would be expected to decrease rapidly when these vibrations freeze out. As can be seen from the data, this is not the fact. Instead, dipolar couplings to surrounding spins modulated by acoustic phonons become visible. This is supported by the fact that the relaxation rates become nearly the same for $N@C_{60}$ and $P@C_{60}$ although the hyperfine and finestructure splittings are one order of magnitude larger for phosphorous than for nitrogen.
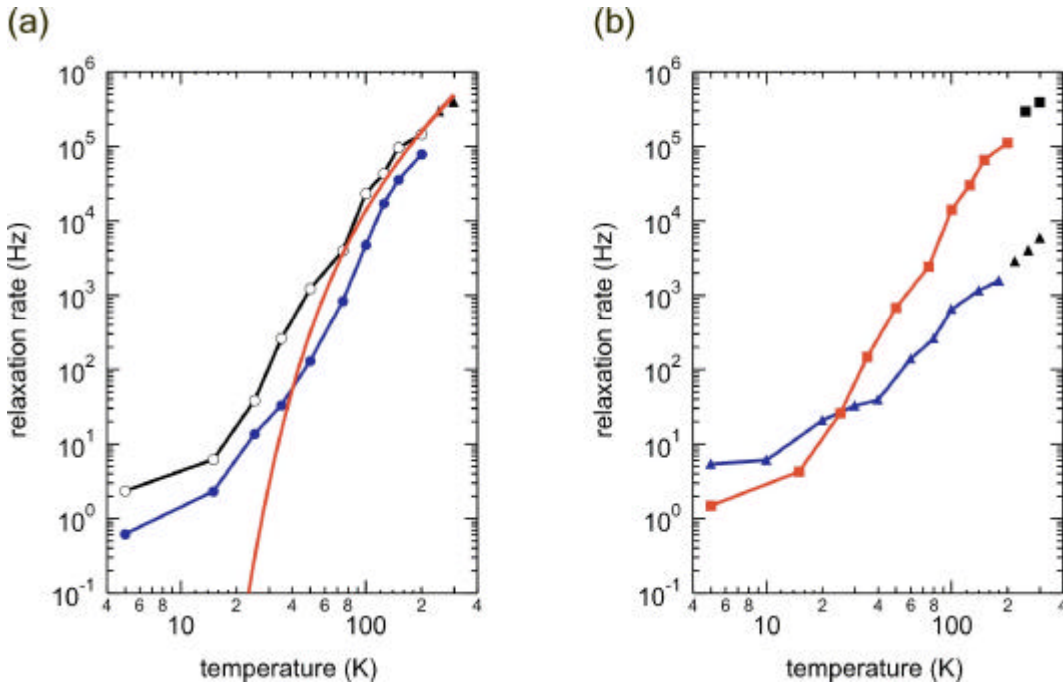

Fig. 3.7:   (a) Temperature dependence of the two spin-lattice relaxation rates evaluated as described in the text. The black line with the open markers corresponds to the hyperfine relaxation R_{hf} and the blue line with the solid markers shows the relaxation due to the fine structure R_{fs}. For $T \geq 250$ K only one relaxation rate is observed (black triangles).The relaxation rates are compared to the modulation of the hyperfine coupling constant Da^2, as expected from theory (red line).

(b)Mean relaxation rate of $P@C_{60}$ (squares) compared to the mean relaxation rate of $N@C_{60}$ (triangles).The data points with a mono–exponential decay have black markers. Data for $N@C_{60}$ are taken from [2].

In the case of anisotropic dipolar coupling a multi–exponential decay is expected. Unfortunately, the time dependent data cannot be fitted with the fixed amplitudes and arguments of the exponential functions calculated in [3]. Instead, the decay of the magnetisation could be described by a stretched exponential function

$$m_z(t) = 1 - \exp[-(t \cdot R)^b]$$ (3.18)

with $\beta \sim 0.5$ for $T \leq 35$ K for phosphorous indicating a broad distribution of relaxation rates. Nevertheless, the coupling strength has to be the same for nitrogen and

phosphorous, as expected from dipolar couplings to surrounding nuclear spins of ^{13}C or endohedral spins and, perhaps, other paramagnetic impurities.

The relaxation at T ≤ 35 K is therefore expected to depend on spin concentration, crystallite size, sample preparation and purification. Some variations of T_l from sample to sample at low temperatures have indeed been observed. No systematic investigation of this phenomenon has been done.

3.3   Spin – spin relaxation

The spin–spin relaxation is perhaps the most important property of a system that is to be used as a qubit in a quantum computer. Because phase coherence is essential in quantum computation, T_2 is the limit for the length of an algorithm.

The real part (a) and the imaginary part (b), blue line, of the echo amplitude of the Hahn–Echo experiment done at T = 100 K are shown in Fig. 3.8. In contrast to the spin–lattice relaxation, the spin–spin or transverse relaxation shows a single exponential behaviour. As can be clearly seen in Fig. 3.8 (b), the residuum of the fit with a single exponential decay (red line) follows the imaginary part of the signal corresponding to the signal noise.
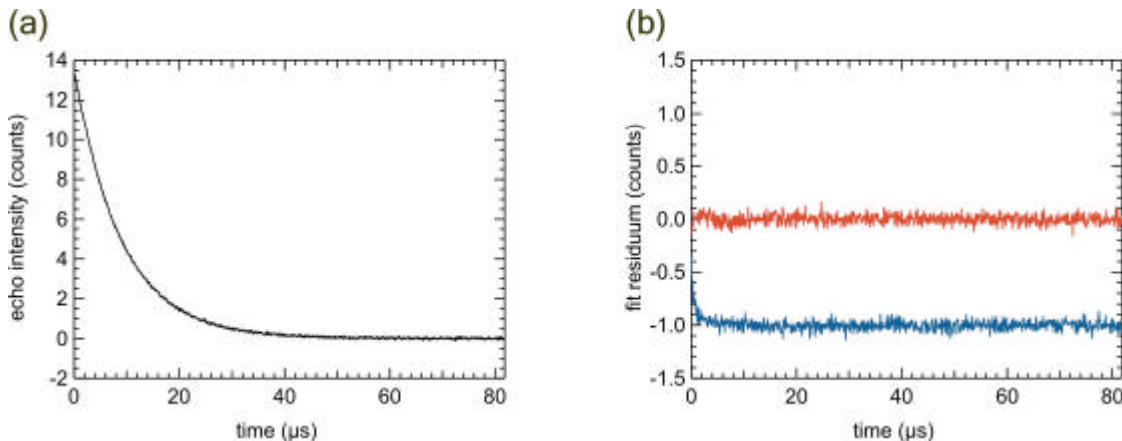

Fig. 3.8:   (a) Echo amplitude measured in a Hahn-Echo experiment at T = 100 K.

(b) Residuum of the spin–spin relaxation fitted with a single exponential decay (red) compared to the imaginary part (blue) corresponding to the signal noise. It can be clearly seen that a simple exponential function describes the data well.

In Fig. 3.9, the temperature dependence of T_2 (solid blue markers) and the mean spin–lattice relaxation time $T_l = 1/R_{mean} = 2/(R_{hf} + R_{fs})$ (see page 34) measured for the sample "Phoenix" is shown. The T_2 relaxation is influenced by T_l for T > 35 K and reaches the limit of $2 \cdot T_2 = T_1$ at room temperature. However, at low temperatures T < 35 K the spin-spin relaxation time is not longer affected by T_l but becomes constant with $T_2 = 14$ µs. So it can be said that T_2 of $P@C_{60}$ itself is temperature independent as it is for $N@C_{60}$ [2], and the process that gives rise to dephasing has to be temperature independent as well.

From N@C$_{60}$ it is already known that the (temperature independent) dipolar coupling between two endohedral electron spins affects the ESR linewidth i. e., the linewidth increases linearly with increasing spin concentration [9]. The T$_2$ relaxation time is anti–proportional to the linewidth and therefore decreases with higher spin concentrations.
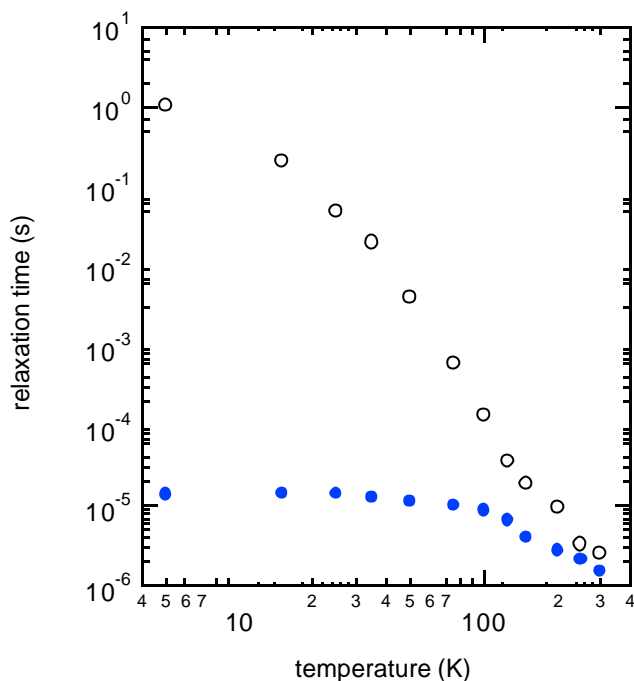

Fig. 3.9:   *Temperature dependence of the spin-spin relaxation time T_2 (solid blue markers) and the mean spin-lattice relaxation time T_1 (open black markers). The T_2 relaxation is constant for $T < 35$ K and dominated by T_1 for $T > 35$ K. At $T = 298$ K the spin-spin relaxation time reaches the limit of $2 \times T_2 = T_1$.*

A similar process seems to be valid for P@C$_{60}$. In a sample with high spin concentration (ratio of filled to empty cages $\sim 10^{-4}$) the spin–spin relaxation time was as short as T$_2$ = 1 µs even at T = 10 K. At a small spin concentration ($\sim 10^{-6}$) T$_2$ was increased up to T$_2$ = 28 µs indicating that the measurement still does not reveal the true relaxation time for a spin system in the "infinite dilution" limit, where coupling to other P@C$_{60}$ molecules is ineffective.

3.4   Conclusions

The properties of fullerenes in solid state remain mainly molecular. In this chapter it has been shown that this is also true for the group–V endohedral fullerenes. The relaxation is dominated by the "inner" modes of the molecule in a large temperature regime.

The spin–lattice relaxation is caused by fluctuations of the hyperfine and fine structure coupling due to vibrations of the endohedral atom in the C$_{60}$ shell. This explains why the relaxation rate is much larger for P@C$_{60}$ than for N@C$_{60}$. Due to the larger overlap of the wavefunctions of the endohedral atom and the fullerene molecule, the fluctuations of the couplings are stronger in P@C$_{60}$.

For temperatures T > 35 K the temperature dependence of these fluctuations is well described by a harmonic oscillator mode, as evidenced by a comparison to the experimental temperature dependence of the hyperfine coupling shown in chapter 2. However, at temperatures T < 35 K this model would lead to much smaller relaxation rates than measured in the experiments. In this case, other interactions and external phonon modes take over the relaxation process.

The strength of these interactions is modulated by acoustic phonons and has to be the same for phosphorous and nitrogen in C_{60}. This condition is fulfilled by dipolar couplings to ^{13}C nuclear spins on neighbouring molecules and other endohedral spins. The coupling to ^{13}C spins $T/2\pi h \sim 70$ kHz is much stronger than the dipolar coupling between endohedral electron spins in as produced material ($J/2\pi h \sim 1$ kHz). When the electron spin concentration reaches $\sim 0.2\%$, both interactions will be of same strength.

For pure $P/N@C_{60}$, the dipolar coupling between adjacent endohedral spins is 50 MHz. As the fine structure coupling of both endohedral fullerenes is smaller, $D/2\pi h \sim 14$ MHz for $P@C_{60}$, one might expect that in this case dipolar interaction will play a major role in the relaxation process. But as it is modulated by acoustic phonons, the temperature dependence has to fit in the Debye model of density of states. Therefore, the relaxation resulting from fluctuations of the dipolar coupling will always be much smaller[8] than those modulated by harmonic oscillations.

All known relaxation times of $N@C_{60}$ and $P@C_{60}$ are listed in Tab. 3.2:

Tab. 3.2: Relaxation times of group-V endohedral fullerenes [2],[6], [11]

Endohedral fullerene	Relaxation in solution		Relaxation in solid C_{60}		Relaxation in solid C_{60}[a]	
	T_1 (µs)	T_2 (µs)	T_1 (µs)	T_2 (µs)	T_1 (µs)	T_2 (µs)
$^{14}N@C_{60}$	120	50	120	20	$\geq 10^6$	20
$^{15}N@C_{60}$	Not measured		≈ 45	11	$\geq 10^6$	14
$^{31}P@C_{60}$	5	3	2.7[b]	1.3[b]	$\geq 10^{6}$[b]	14[b] – 28[b]

[a] At $T = 5$ K. All other values are given for room temperature.
[b] measured in this work

The spin–spin relaxation T_2 depends on the spin concentration and is temperature independent. T_2 is affected by the spin–lattice relaxation at T > 35 K for $P@C_{60}$ and $^{15}N@C_{60}$, though in the latter case the effect is very small. The relaxation time T_2 increases with decreasing spin concentration. Relaxation times up to $T_2 = 28$ µs (for spin concentration $\sim 10^{-6}$) have been measured.

---

[8] even if Raman processes are taken into account

This shows that the "infinite dilution" limit is still not reached at this spin concentration and spin–"flipflops" due to dipolar interactions are dominating the transversal relaxation. The dipolar coupling will be controlled in a quantum computing scheme, so that it can be turned on an off. Therefore, the dephasing time of the quantum computing system will be longer than 28 μs and might even reach T_1 as an absolute limit.

As long as the dipolar coupling is controlled, neither the spin–lattice relaxation nor the spin–spin relaxation will increase with increasing spin concentration. In case of a solid state quantum computer, this means that additional qubits do not cause additional dephasing. Since relaxation is mainly due to fluctuations of the hyperfine and finestructure coupling, and since these values vary only slightly for endohedral adducts, no essential change of the relaxation is expected when chemical modifications of C_{60} are employed, as is planned for the quantum register (see chapter 1). Thus, a quantum computer built from endohedral fullerenes will be scalable.

For temperatures $T > 35$ K, the relaxation is well understood. A detailed analysis at low temperatures, however, would require more data about different samples concerning spin concentration, crystallite size, sample preparation and purification. At the present state of research, more information about the relaxation at low temperatures is not essential for the use of endohedral fullerenes for quantum computing and thus were not in the focus of this work. Much more important is the knowledge about the spin properties concerning single qubit operations, which will be discussed in the next chapter.